HHS Public Access

Author manuscript

Science. Author manuscript; available in PMC 2016 January 12.

Published in final edited form as:

Science. 2015 May 1; 348(6234): 589–594. doi:10.1126/science.aaa7017.

Regulatory T cells generated early in life play a distinct role in maintaining self-tolerance

Siyoung Yang[*,1,2], **Noriyuki Fujikado**[*,1], **Dmitriy Kolodin**[1], **Christophe Benoist**[†,1,3], and **Diane Mathis**[†,1,3]

[1]Division of Immunology, Department of Microbiology and Immunobiology, Harvard Medical School, Boston, MA 02115

[2]Aging Intervention Research Center, Korea Research Institute of Bioscience and Biotechnology (KRIBB), 125 Gwahak-ro, Yuseong-gu, Daejeon, 305-806, South Korea

[3]Evergrande Center for Immunologic Diseases, Harvard Medical School and Brigham and Women's Hospital, Boston MA 02115, USA

Abstract

Aire is an important regulator of immunological tolerance, operating in a minute subset of thymic stromal cells to induce transcripts encoding peptides that guide T-cell selection. Expression of Aire during a perinatal age-window is necessary and sufficient to prevent the multi-organ autoimmunity characteristic of Aire-deficient mice. We report that Aire promotes the perinatal generation of a distinct compartment of $Foxp3^+CD4^+$ regulatory T (Treg) cells, which stably persists in adult mice. This population has a role in maintaining self-tolerance, transcriptome and activation profile distinguishable from those of Tregs produced in adults. Underlying the distinct Treg populations are age-dependent, Aire-independent differences in the processing and presentation of thymic stromal-cell peptides, resulting in different T-cell receptor repertoires. Our findings expand the notion of a developmentally layered immune system.

Individuals with APECED (autoimmune polyendocrinopathy-candidiasis-ectodermal dystrophy) have a mutation in the gene encoding Aire. Such individuals, and mice lacking Aire, develop multi-organ autoimmune disease. Aire promotes immunological tolerance by inducing, specifically in thymic medullary epithelial cells (MECs), a large repertoire of mRNA transcripts encoding proteins characteristic of differentiated cell-types (peripheral-tissue antigens, PTAs), such as insulin or casein-α. Peptides derived from these proteins are displayed on major histocompatibility complex (MHC) molecules at the MEC surface. The MHC:PTA-peptide complexes negatively select thymocytes whose antigen (Ag) receptors (T cell receptors, TCRs) are engaged too aptly. In addition, MECs can positively select

---

[†]Correspondence to: cbdm@hms.harvard.edu.
[*]These authors contributed equally to this work

Supplementary Materials
Materials and Methods
Figs. S1 to S12
Tables S1, S2
References 32–42

Foxp3$^+$CD4$^+$ regulatory T (Treg) cells (1, 2), at least some of them in an Aire-dependent manner (3, 4). Cross-presentation of Aire-induced PTAs by thymic dendritic cells (DCs) also occurs, and can promote either negative or positive selection (4, 5). Aire's presence during the first few weeks of life is necessary and sufficient to guard against the autoimmune disease characteristic of *Aire*-knockout (KO) mice (6). We sought to uncover the root of this unexpected finding.

To compare the effectiveness of clonal deletion in perinatal and adult mice, we examined the thymus of young and old *Aire*-WT and *Aire*-KO animals expressing 1) membrane-bound ovalbumin driven by the rat insulin promoter (RIP-mOva), and thereby within MECs; and 2) TCRs that recognize a peptide of ovalbumin presented by MHC-II molecules (OT-II) (7, 8). In both perinatal and adult mice, Aire-dependent clonal deletion was readily evident (Fig. S1).

As a first step in comparing the Treg compartments, we enumerated Foxp3$^+$CD4$^+$ T cells in the thymus of progressively older *Aire*-WT and -KO mice (Figs. 1A and S2A). While a few Tregs were detected in the thymus of WT individuals two days after birth, a substantial population was evident only on day 4, and it gradually increased through day 35. KO mice showed a similar pattern of Treg accumulation in the thymus, but their fractional representation was reduced *vis-à-vis* WT littermates through day 35, and their numbers until day 10. Results were similar in the periphery (Fig. S2B and A).

To address the relative importance of the Treg compartments for the maintenance of immunological tolerance, we used a NOD.*Foxp3-DTR* system to deplete Tregs during the day 0–10 or day 35–45 age-window, and followed the mice until fifteen weeks of age (or loss of ≥ 20% body weight). Depletion of Tregs during the 0–10 day window resulted in significant weight reduction by 16 days of age (even though Treg numbers were normal by day 11–12), and ≥20% weight loss in all mice by 24 days (Fig. 1B). All individuals showed the multi-organ autoimmunity typical of *Aire*-KO mice on the NOD genetic background (Figs. 1B and S3). In contrast, Treg ablation during the 35–45 day window had no significant effect on either weight gain or survival, although there were some mild manifestations of autoimmunity in scattered individuals (Figs. S4 and S3).

We next performed a complementation experiment to rule out the trivial explanation that perinatal mice are non-specifically perturbed by the repeated injection of DT. Addition of Tregs from 20-day-old Treg-replete, but not Treg-depleted, donors to recipients perinatally depleted of Tregs resulted in a striking improvement in the autoimmune manifestations (Figs. S5 and S6). To confirm that the critical perinatally generated Treg population was, indeed, Aire-dependent, we transferred Tregs isolated from 20-day-old *Aire*-WT or -KO mice into either Treg-depleted (Fig. 1C and D) or *Aire*-KO (Fig. S7) perinates. For both types of recipient, only the perinatal Tregs from WT mice protected from development of the characteristic "Aire-less" autoimmune disease. Thus, Aire promotes the generation of Treg cells during the perinatal age-window. Mice lacking these cells phenocopy *Aire*-KO mice; exhibiting a spectrum of pathology that differs substantially from that of mice either constitutively lacking Tregs or depleted of them as adults (9–11).

An inducible Treg lineage-tracer system (12) allowed us to explore the functional and phenotypic properties of perinatally generated Tregs. In NOD-backcrossed Foxp3$^{eGFP\text{-}Cre\text{-}ERT2}$xR26Y mice, all Foxp3^{+}CD4^{+} cells express GFP; treatment with tamoxifen turns on yellow fluorescent protein (YFP) in the Tregs extant during drug coverage, rendering them GFP/YFP double-positive thereafter. We first used this system to examine the stability of Tregs made perinatally. Lineage-tracer mice were injected with tamoxifen from days 0–10 or 35–45, and their splenic Treg compartment analyzed 1 day, 1 week or 8 weeks later (Fig. 2). The adult-tagged and perinate-tagged Treg populations were both readily discernible the day after termination of tamoxifen, constituting about a quarter of the Foxp3^{+}CD4^{+} compartment. For adult-tagged Tregs, this fraction remained similar throughout the period examined. In contrast, perinate-tagged Tregs dwindled to a minor component of the Foxp3^{+}CD4^{+} compartment between 1 and 8 weeks after cessation of labeling. This reduction in fractional representation was a dilution effect as total Treg numbers increased exponentially during this time. In fact, the actual numbers of perinate-tagged Tregs was very stable over the two months examined.

The persistence of the tagged Treg populations permitted us to address the functionality of perinatally generated Tregs by conducting a four-way comparison (as schematized in Fig. S8A). Mice were treated with tamoxifen from 0–10 or 35–45 days, and were then left unmanipulated until 60 days of age, at which time the GFP^{+}YFP^{+} (tagged) Treg and GFP^{+}YFP^{-} (bulk) Treg populations were sorted and transferred into newborn *Aire*-KO mice. According to all criteria evaluated, disease was not affected by introduction of adult-tagged Tregs nor either control bulk Treg population (Figs. 2B–D and S8B). In contrast, addition of perinate-tagged Tregs resulted in substantial reversal of the typical *Aire*-KO pathology (but with substitution of the insulitis characteristic of classical NOD mice) (Figs. 2E and S8B). These findings argue that the Treg population generated perinatally has distinct functional properties that persist within the adult environment.

We also sorted GFP^{+}YFP^{+} and GFP^{+}YFP^{-} CD4^{+} T cells from 8–10 week-old mice whose Tregs had been labeled between 0 and 10 or 35 and 45 days after birth, and analyzed their transcriptomes. Distinct sets of genes were either over- (pink) or under-expressed (green) in Treg cells tagged perinatally *vis-à-vis* the bulk Treg population of the same mice, but were not differentially transcribed in mice whose Tregs were labeled as adults (Fig. 3A, Table S1). Overlaying the standard Treg signature on a volcano plot comparing the two labeled Treg populations revealed an over-representation of Treg “up” genes in perinate-tagged Tregs (Fig. 3B). Indeed, these Tregs performed better than the three comparator populations in a typical *in vitro* suppression assay (Fig. 3C), perhaps reflecting higher transcription of genes such as *Fgl2*, *Ebi3*, *Pdcd1*, *Icos*, etc (Table S1A), previously implicated in Treg effector function (13–16). The perinate-tagged Treg population was in a more activated state (Fig. 3D), which fit with its higher content of CD44^{hi}CD62L^{lo} cells (Fig. 3E). It was also more proliferative, as indicated by fractions of EdU-incorporating and of Ki67^{+} cells higher than those of the three comparator populations (Fig. 3F). Indeed, the top pathways over-represented in perinate-tagged Tregs according to Gene-Set Enrichment Analysis (GSEA) were related to DNA replication and cell division (eg, Fig. 3G). We confirmed the elevated expression of a number of functionally relevant genes at the protein level (Figs. 3H and S9).

Lastly, we sought a molecular or cellular explanation for the distinct Treg compartments generated in perinatal and adult mice. We first used a mixed fetal-liver:bone-marrow chimera approach to rule out the possibility that T cell precursors derived from fetal liver hematopoietic stem cells, which service the developing immune system for the first few weeks after birth (17), are predisposed to yield Tregs with particular properties, measuring both reconstitution efficiencies and gene-expression profiles (Fig. S10).

To facilitate comparison of the repertoires of Aire-dependent PTA transcripts in perinatal and adult MECs, we generated Adig reporter mice, which express GFP under the dictates of *Aire* promoter/enhancer elements (18), on either an *Aire*-WT or -KO background. $GFP^{+}MHC\text{-}II^{hi}$ cells were isolated from thymic stroma of <3-day-old or 5-week-old animals, and gene-expression profiling performed. The fraction of $Aire^{+}MHC\text{-}II^{hi}$ MECs and the Aire mean fluorescence intensity (MFI) were indistinguishable in mice of the two ages (Fig. S11A and B). The repertories of Aire-dependent MEC transcripts were also extremely similar (Fig. S11C).

Going one step further, we asked whether the similar repertoires of PTA transcripts might still yield distinct sets of MHC-presented peptides, owing to different Ag-processing/presentation machinery in mice of the two ages, which need not be Aire-dependent. Transcripts encoding several molecules implicated in generating or regulating the repertoire of peptides bound to MHC-II or -I molecules were differentially expressed in perinatal and adult MECs (Fig. 4A and data not shown). The data on *H2-O* transcripts drew our attention because DO is known to inhibit the activity of DM, an “editor” needed for dislodging the invariant chain (CD74) derivative, CLIP, and other peptides from the Ag-binding groove of a maturing MHC-II molecule, enabling effective loading of a diverse repertoire of peptides (19, 20). Transcripts encoding both DO chains were expressed at a significantly lower level in perinatal than in adult MECs, independently of Aire (Fig. 4B); perinatal MECs also had reduced levels of intracellular DO complexes (Fig. 4C). In addition, they displayed higher intracellular levels of DM complexes (Fig. 4E). Co-plotting intracellular levels of the two complexes at the single-cell level revealed a subset of perinatal MECs with reduced DO and enhanced DM expression (Fig. 4F). A lower DO:DM ratio should promote more effective replacement of CLIP by other peptides. Indeed, a higher percentage of perinatal MECs displayed low levels of or no CLIP (37.6 ± 6.4% vs 20.9 ± 2.2%), and the CLIP MFI was lower for perinatal MECs (761.7 ± 78.7% vs 1019.0 ± 54%) (Fig. 4G). Thus, the repertoires of peptides presented by perinatal and adult MECs are different, the latter appearing to be more limited.

Aire-dependent PTAs can be “cross-presented” by myeloid-lineage cells in the vicinity (4, 5), primarily $MHC\text{-}II^{hi}CD8\alpha^{+}$ DCs (4). Interestingly, this cell-type was present at strongly reduced levels in thymi from perinatal mice (Fig. 4H). Since the splenic $MHC\text{-}II^{hi}CD8\alpha^{+}$ DC subset showed an even more extreme age-dependence, it is unlikely that this difference is Aire dependent.

Such differences in the Ag processing/presentation machinery of MECs from perinatal and adult mice suggested that their Treg TCR repertoires might diverge. We constrained the inventory of TCRs to be examined by using an approach that had proven fruitful in the past

(21, 22). BDC2.5 is a $V_\alpha1^+V_\beta4^+$ T helper cell specificity directed at a pancreatic Ag presented by A^{g7} molecules; so generation of Tregs in BDC2.5/NOD mice is dependent on rearrangement of an endogenous *Tcra* gene and thymic selection on the resulting second TCRαβ complexes. The fixed $V_\beta4^+$ chain constrains the TCR repertoire, and the analysis is further delimited by sorting individual cells expressing $V_\alpha2$. We sequenced 281 $V_\alpha2^+$ TCR CDR3 regions from splenic Tregs of 3 individual BDC2.5/NOD adults and another 232 from the corresponding population of 3 individual perinates. This restricted, but parallel, slice of the TCR repertoire was clearly different in the two age-groups. Perinate Treg TCRs were less clonally expanded (Fig. S12A), had shorter CDR3α stretches (Fig. S12B) and, as expected (23), had fewer *Tcra* N-region additions (Fig. S12C). To permit a more statistically robust assessment, we focused on repeat sequences. There were many more repeated sequences in the adult mice, and very low values were obtained for both the Morisita-Horn Index (0.069 on a scale from 0–1) and the Chao abundance-based Jaccard index (0.058 on a scale from 0–1), indicating that the two repertoires were very different (Table S2 and Fig. 4I).

Thus, our data highlight Aire's ability to promote the generation of a distinct compartment of $Foxp3^+CD4^+$ Tregs as the explanation for its importance during the perinatal age-window. Given the age-dependent differences in antigen processing machinery and presenting cells we documented, juvenile and older mice are likely to have distinct repertoires of both Aire-dependent and Aire-independent Tregs, selected primarily on Ag:MHC complexes encountered on MECs. These findings add to, rather than negate, Aire's role in clonal deletion of self-reactive thymocytes, established in multiple experimental contexts (4, 5, 24, 25).

There are striking similarities in the autoimmune diseases provoked by constitutive genetic ablation of *Aire*, thymectomy at 3 days of age, and perinatal depletion of Foxp3-expressing cells in particular, the pattern of target tissues on different genetic backgrounds ((26, 27) and Fig. 1). Our studies yield a unifying explanation for these phenocopies: the perinatally generated, Aire-dependent Treg compartment is particularly apt at protecting a defined set of tissues from autoimmune attack, and there may be little overlap with the tissues guarded by adult Tregs. This notion is consistent with the observations that mice which underwent a thymectomy 3 days after birth exhibit multi-organ autoimmune disease but do not have a numerically diminished Treg compartment when they get older (28, 29), and that mice constitutively devoid of Tregs or inducibly depleted of them as adults show a very different spectrum of pathologies (9–11). Such a dichotomy also provides an explanation for the frequently posed question: why is the autoimmune disease characteristic of both APECED patients and *Aire*-KO mice restricted to such a limited set of tissues? An important implication of this dichotomy is that therapies based on transfer of Tregs isolated from adult donors may not be able to impact a particular subset of autoimmune diseases. Thus, our findings extend the notion of a "layered" immune system (30).

MATERIALS and METHODS

Mice

B6.*Aire*-KO and NOD.*Aire*-KO mice (26), OT-II TCR-transgenic mice (7), and NOD.*Foxp3-DTR* mice (32) were maintained in our colony housed at Jackson Laboratory. RIP-mOVA transgenic mice (33) were received from Dr. Andrew Lichtman. *Igrp-Gfp* (*Adig*) mice (18) were provided by Dr. Mark Anderson, and were appropriately bred to yield *Aire*-WT and *Aire*-KO littermates. Foxp3$^{eGFP\text{-}Cre\text{-}ERT2}$ X R26Y mice on a mixed Sv129// C57Bl/6 genetic background (12) were obtained from Dr A. Rudensky, and were backcrossed 10 generations onto the NOD background.

For *in vivo* depletion of Treg cells, NOD.*Foxp3-DTR*$^{+}$ mice or NOD.*Foxp3-DTR*$^{-}$ control littermates were injected ip with DT (Sigma) (50 ng/g body weight, every other day) from day 0–10 or 35–45 after birth. In some experiments, control mice were NOD.*Foxp3-DTR*$^{+}$ mice administered phosphate-buffered saline (PBS). To induce GFP^{+}YFP^{-} or GFP^{+}YFP^{+} populations for microarray analysis, lineage-reporter mice were injected ip with tamoxifen (4 injections, every third day) between 0–10 (perinate) or 35–45 (adult) days of age, and were keep until 8 wks of age. For quantification of *in vivo* T cell proliferation, 1mg EdU was injected ip; 24hrs later cells were processed.

All mice were housed and bred under specific pathogen-free conditions at the Harvard Medical School Center for Animal Resources and Comparative Medicine (Institutional Animal Care and Use Committee protocol 2954).

Antibodies and flow cytometry

Antibodies used for staining were as follows: anti-CD3, -CD4, -CD8, -CD25, -CD44, -CD45, -CD62L, -ICOS, -PD1, -TIM3, -Ly51, -MHC-II A/E, -Vα2 (B20.1), and -Vβ5 (MR9-4) (all BioLegend); anti-Fgl2 (Bioss); anti-CCR2, -CXCR3, -EBI3 and -ST2 (all R&D); anti-Foxp3 (eBiosciences); anti-Ki67, -DM (BD Pharmingen); and anti-DOb (M-15), -A^{b}/CLIP (30.2) (Santa Cruz). Intracellular expression of Foxp3, Ki67 and DM and DOb was determined using the Intracellular Fixation & Permeabilization buffer set (eBiosience) according to the manufacturer's protocol. EdU detection was done after the last wash with permeabilization buffer following the Click-iT EdU kit (Molecular Probes) instructions. Flow cytometric analysis was performed on an LSR II, sorting on a FACSAria (BD Bioscience), or on a MoFlo (Beckman Coulter) and data were analyzed using FlowJo software (Tree Star).

Microarray analysis

MECs were isolated from adult (5 weeks old) or perinatal (0–3 days old) *Aire*-WT or *Aire*-KO *Adig* mice by double-sorting as described in (34).

Perinate-tagged or adult-tagged GFP^{+}YFP^{+} cells and bulk GFP^{+}YFP^{-} cells from the same mice were double-sorted into Trizol (Invitrogen) after ip injection of tamoxifen from 0–10 (perinate) or 35–45 (adult) days of age. All samples were generated in triplicate. RNA

amplification and microarray hybridization were done as previously described (35, 36). Pathway analysis was performed using web-based tools, e.g GSEA

Treg-transfer analyses

For the complementation experiments of Fig. S4: Treg cells from the spleen of NOD.*Foxp3.DTR*$^+$ mice treated with DT or PBS from 0–10 days after birth were isolated at 20 days of age by flow cytometry (GFP$^+$CD4$^+$CD3$^+$), and 3 x 10^5 were injected ip into DT-treated (from 0–10 days) perinates at 12 and 19 days of age. For the comparison of perinate-tagged and adult-tagged Treg function: GFP$^+$YFP$^+$ tagged and GFP$^+$YFP$^-$ bulk cells were purified from 60-day-old mice labeled from 0–10 or 35–45 days of age via negative selection of non-T cells (Miltenyi Biotech) followed by sorting (GFP$^+$YFP$^-$CD4$^+$ or GFP$^+$YFP$^+$CD4$^+$). 1.5 x 10^5 purified Treg cells were injected ip into Aire-deficient mice at 0.5, 3 and 7 days after birth. For the analysis of Aire-dependence: 1.5 – 3.0 x 10^5 Treg cells were isolated from spleens of 20-day-old *Aire*-WT or -KO mice by negative selection and sorting (CD3$^+$CD4$^+$CD25$^+$), and were injected ip into DT-treated perinates at 12 and 19 days of age or *Aire*-KO mice at 0.5, 3 and 7 days of age.

Mixed bone-marrow and fetal-liver chimera experiments

Hematopoietic progenitor cells (3 X 10^6) were isolated from E18.5 fetal liver of B6.CD45.1 mice or from bone marrow of 5 wk-old B6.CD45.2 mice via negative selection of Thy1.2$^+$ cells (Miltenyi Biotech). The two populations were mixed at a 1:1 ratio, and were iv-transferred into irradiated (1000 rad) RAG-1−/− mice (6–8 wks of age). 4 wks after irradiation, antibiotic treatment was stopped until flow cytometric analysis at 6 or 12 weeks of age.

Histopathology

Histopathology was assessed as previously described (37). Briefly, we weighed mice three times per week and sacrificed them when they had lost 15–20% body weight relative to littermate controls. Tissues were fixed in 10% formalin, embedded with paraffin, and stained with hematoxylin and eosin. Infiltration scores of 0, 0.5, 1, 2, 3 and 4 indicate no, trace, mild, moderate, or severe lymphocytic infiltration, and complete destruction, respectively. For retinal degeneration: 0 = lesion present without any photoreceptor layer lost; 1 = lesion present, but less than half of the photoreceptor layer lost; 2 = more than half of the photoreceptor layer lost; 3 = entire photoreceptor layer lost without or with mild outer nuclear layer attack; and 4 = the entire photoreceptor layer and most of the outer nuclear layer destroyed. All infiltrated samples were scored blindly by two independent investigators.

AutoAb production

AutoAb production was measured as previously described (26).

In vitro Treg suppression analysis

Splenocytes were depleted of non-T cells *via* negative selection (Miltenyi Biotech). Perinate-tagged or adult-tagged GFP^+YFP^+ cells and bulk GFP^+YFP^- cells from the same mice were sorted. Suppression assays were as per (38).

Single-cell sorting and TCR sequence analysis

Spelnocytes were first sorted in bulk as BDC2.5 clonotype-expressing (39), $V\alpha2^+CD4^+GFP^+$ cells from female BDC2.5/NOD.Foxp3-I-GFP mice at 5 weeks (adult) or 4 days (perinate) of age, before resorting as individual cells into 96-well plates containing the reverse transcriptase reaction mix. cDNA was prepared as described (35, 40, 41). PCR products encoding TCRα chains were subjected to automated sequencing (Dana-Farber/ Harvard Cancer Center High-Throughput Sequencing Core). Raw sequencing files were filtered for sequence quality, processed in automated fashion, and parsed using IMGT/V-QUEST (42).

Statistical analyses

Data were routinely presented as mean ± SD. Significance was evaluated by the Student's t test. The log-rank test was used for the survival rate and a chi-squared test for microarray analysis (volcano plot). Significance was accepted at the 0.05 level of probability ($p < 0.05$). Morisita-Horn Index or Chao abundance-based Jaccard index were determined with EstimateS software (http://viceroy.eeb.uconn.edu/estimates).

Supplementary Material

Refer to Web version on PubMed Central for supplementary material.

Acknowledgments

We thank Drs. A. Rudensky, M. Anderson and A. Lichtman for providing valuable mouse strains; F. Depis and H-K. Kwon for insightful discussions; A. Ortiz-Lopez, L. Denu and Ms. K. Hattori for technical assistance. The data presented in this paper are tabulated in the main paper and in the supplementary materials. Microarray data can be found at GEO #GSE66332 and #xxxxxx. This work was supported by National Institutes of Health Grant R01 DK060027 (to D.M.). S. Yang, N. Fujikado, and D. Kolodin were supported by fellowships from the National Research Foundation of Korea (NRF-2013M3A9B6076413), Japan Society for the Promotion of Science, and National Science Foundation, respectively.

REFERENCES AND NOTES

1. Aschenbrenner K, et al. Selection of Foxp3(+) regulatory T cells specific for self antigen expressed and presented by Aire(+) medullary thymic epithelial cells. Nat Immunol. 2007; 8:351. [PubMed: 17322887]
2. Hinterberger M, et al. Autonomous role of medullary thymic epithelial cells in central CD4(+) T cell tolerance. Nat Immunol. 2010; 11:512. [PubMed: 20431619]
3. Malchow S, et al. Aire-dependent thymic development of tumor-associated regulatory T cells. Science. 2013; 339:1219. [PubMed: 23471412]
4. Perry JS, et al. Distinct contributions of aire and antigen-presenting-cell subsets to the generation of self-tolerance in the thymus. Immunity. 2014; 41:414. [PubMed: 25220213]
5. Taniguchi RT, et al. Detection of an autoreactive T-cell population within the polyclonal repertoire that undergoes distinct autoimmune regulator (Aire)-mediated selection. Proc Natl Acad Sci U S A. 2012; 109:7847. [PubMed: 22552229]

6. Guerau-de-Arellano M, Martinic M, Benoist C, Mathis D. Neonatal tolerance revisited: a perinatal window for Aire control of autoimmunity. J Exp Med. 2009; 206:1245. [PubMed: 19487417]
7. Anderson MS, et al. The cellular mechanism of Aire control of T cell tolerance. Immunity. 2005; 23:227. [PubMed: 16111640]
8. Materials and methods are available as supplemtary materials on *Science* Online.
9. Fontenot JD, et al. Regulatory T cell lineage specification by the forkhead transcription factor foxp3. Immunity. 2005; 22:329. [PubMed: 15780990]
10. Kim JM, Rasmussen JP, Rudensky AY. Regulatory T cells prevent catastrophic autoimmunity throughout the lifespan of mice. Nat Immunol. 2007; 8:191. [PubMed: 17136045]
11. Chen Z, Benoist C, Mathis D. How defects in central tolerance impinge on a deficiency in regulatory T cells. Proc Natl Acad Sci U S A. 2005; 102:14735. [PubMed: 16203996]
12. Rubtsov YP, et al. Stability of the regulatory T cell lineage in vivo. Science. 2010; 329:1667. [PubMed: 20929851]
13. Shalev I, et al. Targeted deletion of fgl2 leads to impaired regulatory T cell activity and development of autoimmune glomerulonephritis. J Immunol. 2008; 180:249. [PubMed: 18097026]
14. Collison LW, et al. The inhibitory cytokine IL-35 contributes to regulatory T-cell function. Nature. 2007; 450:566. [PubMed: 18033300]
15. Polanczyk MJ, Hopke C, Vandenbark AA, Offner H. Treg suppressive activity involves estrogen-dependent expression of programmed death-1 (PD-1). Int Immunol. 2007; 19:337. [PubMed: 17267414]
16. Gotsman I, et al. Impaired regulatory T-cell response and enhanced atherosclerosis in the absence of inducible costimulatory molecule. Circulation. 2006; 114:2047. [PubMed: 17060381]
17. Jotereau F, Heuze F, Salomon-Vie V, Gascan H. Cell kinetics in the fetal mouse thymus: precursor cell input, proliferation, and emigration. J Immunol. 1987; 138:1026. [PubMed: 2879866]
18. Gardner JM, et al. Deletional tolerance mediated by extrathymic Aire-expressing cells. Science. 2008; 321:843. [PubMed: 18687966]
19. Mellins ED, Stern LJ. HLA-DM and HLA-DO, key regulators of MHC-II processing and presentation. Curr Opin Immunol. 2014; 26:115. [PubMed: 24463216]
20. Poluektov YO, Kim A, Sadegh-Nasseri S. HLA-DO and Its Role in MHC Class II Antigen Presentation. Front Immunol. 2013; 4:260. [PubMed: 24009612]
21. Wong J, Mathis D, Benoist C. TCR-based lineage tracing: no evidence for conversion of conventional into regulatory T cells in response to a natural self-antigen in pancreatic islets. J Exp Med. 2007; 204:2039. [PubMed: 17724131]
22. Nishio J, Feuerer M, Wong J, Mathis D, Benoist C. Anti-CD3 therapy permits regulatory T cells to surmount T cell receptor-specified peripheral niche constraints. J Exp Med. 2010; 207:1879. [PubMed: 20679403]
23. Bogue M, Gilfillan S, Benoist C, Mathis D. Regulation of N-region diversity in antigen receptors through thymocyte differentiation and thymus ontogeny. Proc Natl Acad Sci U S A. 1992; 89:11011. [PubMed: 1438306]
24. Mathis D, Benoist C. AIRE. Ann Rev Immunol. 2009; 27:287. [PubMed: 19302042]
25. Kisand K, Peterson P. Autoimmune polyendocrinopathy candidiasis ectodermal dystrophy: known and novel aspects of the syndrome. Ann N Y Acad Sci. 2011; 1246:77. [PubMed: 22236432]
26. Jiang W, Anderson MS, Bronson R, Mathis D, Benoist C. Modifier loci condition autoimmunity provoked by Aire deficiency. J Exp Med. 2005; 202:805. [PubMed: 16172259]
27. Tung KS, Setiady YY, Samy ET, Lewis J, Teuscher C. Autoimmune ovarian disease in day 3-thymectomized mice: the neonatal time window, antigen specificity of disease suppression, and genetic control. Curr Top Microbiol Immunol. 2005; 293:209. [PubMed: 15981482]
28. Dujardin HC, et al. Regulatory potential and control of Foxp3 expression in newborn CD4+ T cells. Proc Natl Acad Sci U S A. 2004; 101:14473. [PubMed: 15452347]
29. Samy ET, Wheeler KM, Roper RJ, Teuscher C, Tung KS. Cutting edge: Autoimmune disease in day 3 thymectomized mice is actively controlled by endogenous disease-specific regulatory T cells. J Immunol. 2008; 180:4366. [PubMed: 18354156]

30. Herzenberg LA, Herzenberg LA. Toward a layered immune system. Cell. 1989; 59:953. [PubMed: 2688900]
31. Hill JA, et al. Foxp3 transcription-factor-dependent and -independent regulation of the regulatory T cell transcriptional signature. Immunity. 2007; 27:786. [PubMed: 18024188]
32. Feuerer M, Hill JA, Mathis D, Benoist C. Foxp3+ regulatory T cells: differentiation, specification, subphenotypes. Nat Immunol. 2009; 10:689. [PubMed: 19536194]
33. Kurts C, et al. Constitutive class I-restricted exogenous presentation of self antigens in vivo. J Exp Med. 1996; 184:923. [PubMed: 9064352]
34. Giraud M, et al. Aire unleashes stalled RNA polymerase to induce ectopic gene expression in thymic epithelial cells. Proc Natl Acad Sci U S A. 2012; 109:535. [PubMed: 22203960]
35. Burzyn D, et al. A special population of regulatory T cells potentiates muscle repair. Cell. 2013; 155:1282. [PubMed: 24315098]
36. Cipolletta D, et al. PPAR-gamma is a major driver of the accumulation and phenotype of adipose tissue Treg cells. Nature. 2012; 486:549. [PubMed: 22722857]
37. Koh AS, Kingston RE, Benoist C, Mathis D. Global relevance of Aire binding to hypomethylated lysine-4 of histone-3. Proc Natl Acad Sci U S A. 2010; 107:13016. [PubMed: 20615959]
38. D'Alise AM, Ergun A, Hill JA, Mathis D, Benoist C. A cluster of coregulated genes determines TGF-{beta}-induced regulatory T-cell (Treg) dysfunction in NOD mice. Proc Natl Acad Sci U S A. 2011; 108:8737. [PubMed: 21543717]
39. Kanagawa O, Militech A, Vaupel BA. Regulation of diabetes development by regulatory T cells in pancreatic islet antigen-specific TCR transgenic nonobese diabetic mice. J Immunol. 2002; 168:6159. [PubMed: 12055228]
40. Wong J, et al. Adaptation of TCR repertoires to self-peptides in regulatory and nonregulatory CD4+ T cells. J Immunol. 2007; 178:7032. [PubMed: 17513752]
41. Baker FJ, Lee M, Chien YH, Davis MM. Restricted islet-cell reactive T cell repertoire of early pancreatic islet infiltrates in NOD mice. Proc Natl Acad Sci U S A. 2002; 99:9374. [PubMed: 12082183]
42. Brochet X, Lefranc MP, Giudicelli V. IMGT/V-QUEST: the highly customized and integrated system for IG and TR standardized V-J and V-D-J sequence analysis. Nucleic Acids Res. 2008; 36:W503. [PubMed: 18503082]

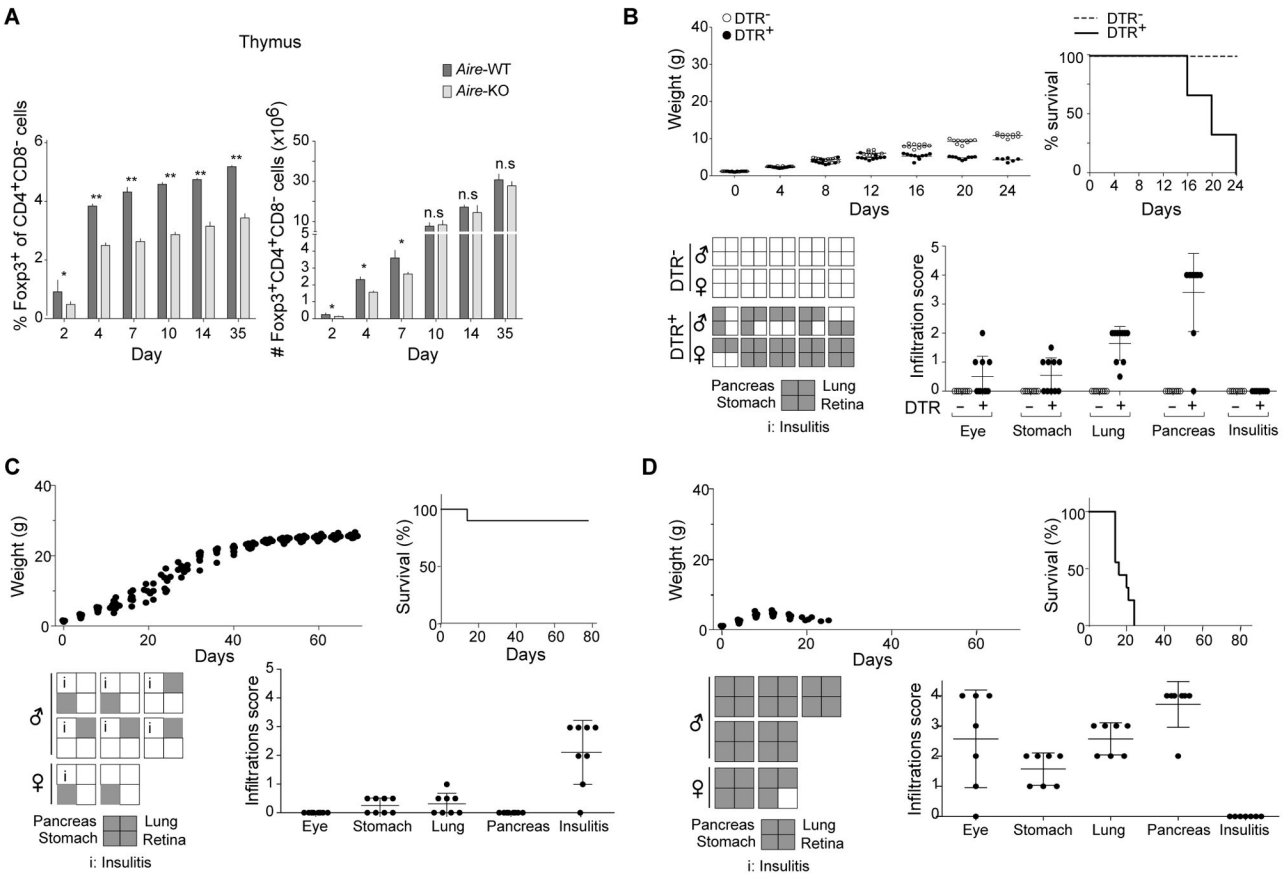

Fig. 1. A perinatal Treg population that is Aire-dependent and guards against the autoimmune manifestations typical of *Aire*-KO mice

(A) Summary data for fractional representation (left) and numbers (right) of $Foxp3^+CD4^+CD8^-$ thymocytes from *Aire*-WT or -KO mice of increasing age. P-values from the Student's t test: *, P≤ 0.05; **≤ 0.01; ns = not significant. n=5. Examples of corresponding dot plots can be found in Fig. S2A. **(B)** Treg depletion in perinates. Perinatal (0.5 days after birth) NOD.*Foxp3-DTR*$^+$ mice or DTR^- littermates were treated every other day until day 10 with DT, and then followed for manifestations of autoimmune disease. Perinates had to be examined <24 days after birth due to wasting in the DTR^+ littermates. Upper left: weight curves. Upper right: survival curves; mice were sacrificed if their weight fell to <20% of that of their DTR^- littermates. Lower left: presence (shaded) or absence of organ infiltrates; "i" indicates that insulitis replaced infiltration of the exocrine pancreas. Lower right: severity of organ infiltration (scored as per the Methods section). n=9. **(C and D)** NOD.*Foxp3.DTR*$^+$ mice perinatally depleted of Tregs as per panel B were supplemented on days 12 and 19 with Tregs isolated form 20-day-old *Aire*-WT (C) or -KO (D) littermates. Cohorts were followed until 70 days of age. n = 9. Otherwise set up as per panel B.

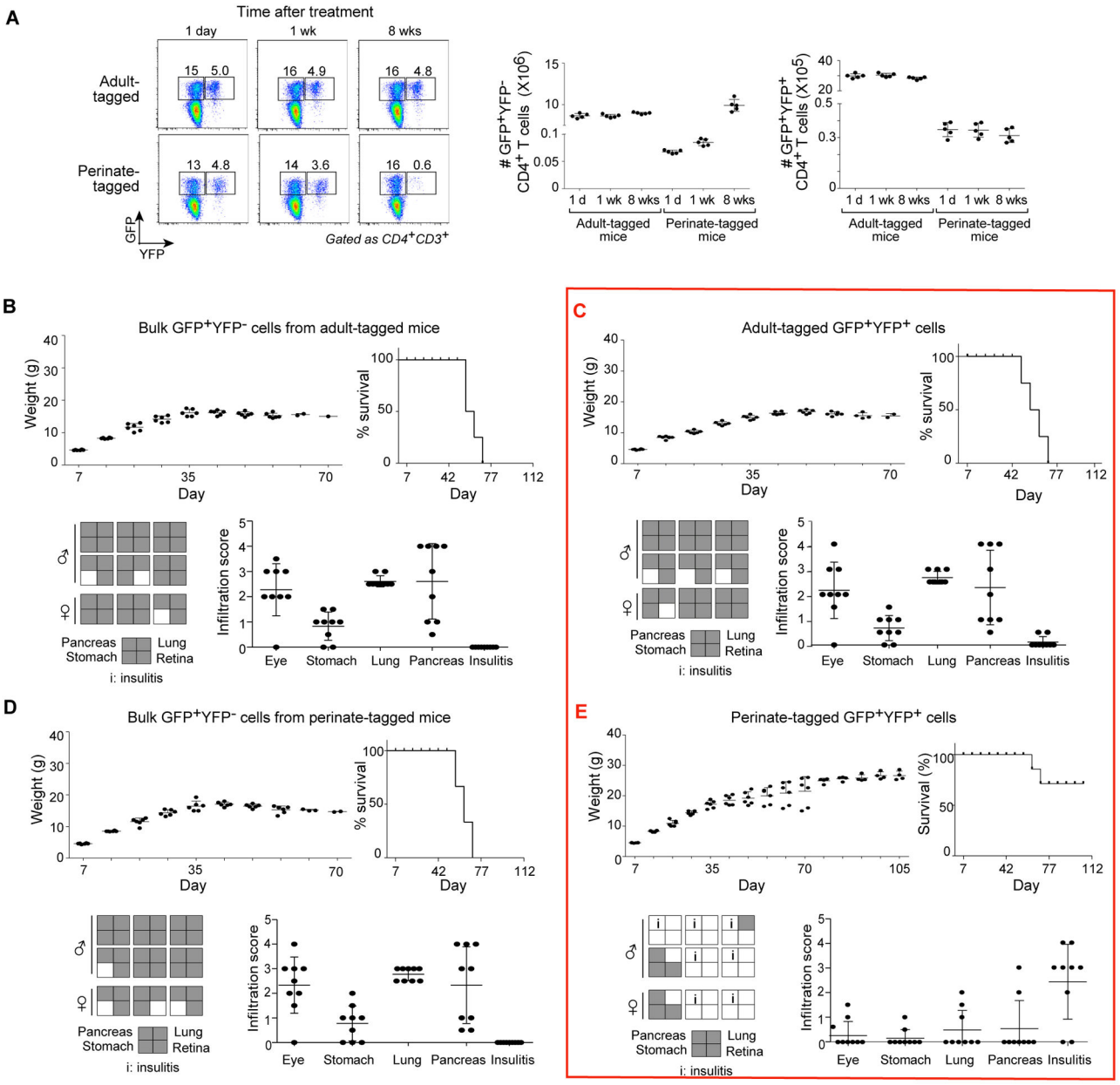

Fig. 2. Stability and function of perinate- versus adult-tagged Tregs

(A) Tamoxifen was administered from 0–10 or 35–45 days of age; at various times later, splenocytes were analyzed for GFP and YFP expression by flow cytometry. Left: representative flow-cytometric dot-plots. Numbers represent percentages of $CD4^+3^+$ cells in the designated gates. Center: summary data on numbers of GFP^+YFP^- bulk Tregs. Right: corresponding data on GFP^+YFP^+ perinate-tagged or adult-tagged Tregs from the same mice. n=5. **(B–E)** $1.5x10^5$ Tregs were transferred into *Aire*-KO mice on days 0.5, 3 and 7 after birth, and the recipients were followed until 16 weeks of age. A four-way comparison as schematized in Fig. S8A: GFP^+YFP^+ Tregs tagged from 35–45 days of age and isolated from a 60-day-old mouse (C), GFP^+YFP^- bulk Tregs from the same mouse (B), GFP^+YFP^+ Tregs tagged from 0–10 days of age and isolated from a 60-day-old mouse (E), and

GFP^+YFP^- bulk Tregs from the same mouse (D). Data organized as per Fig. 1B. The key comparison is boxed.

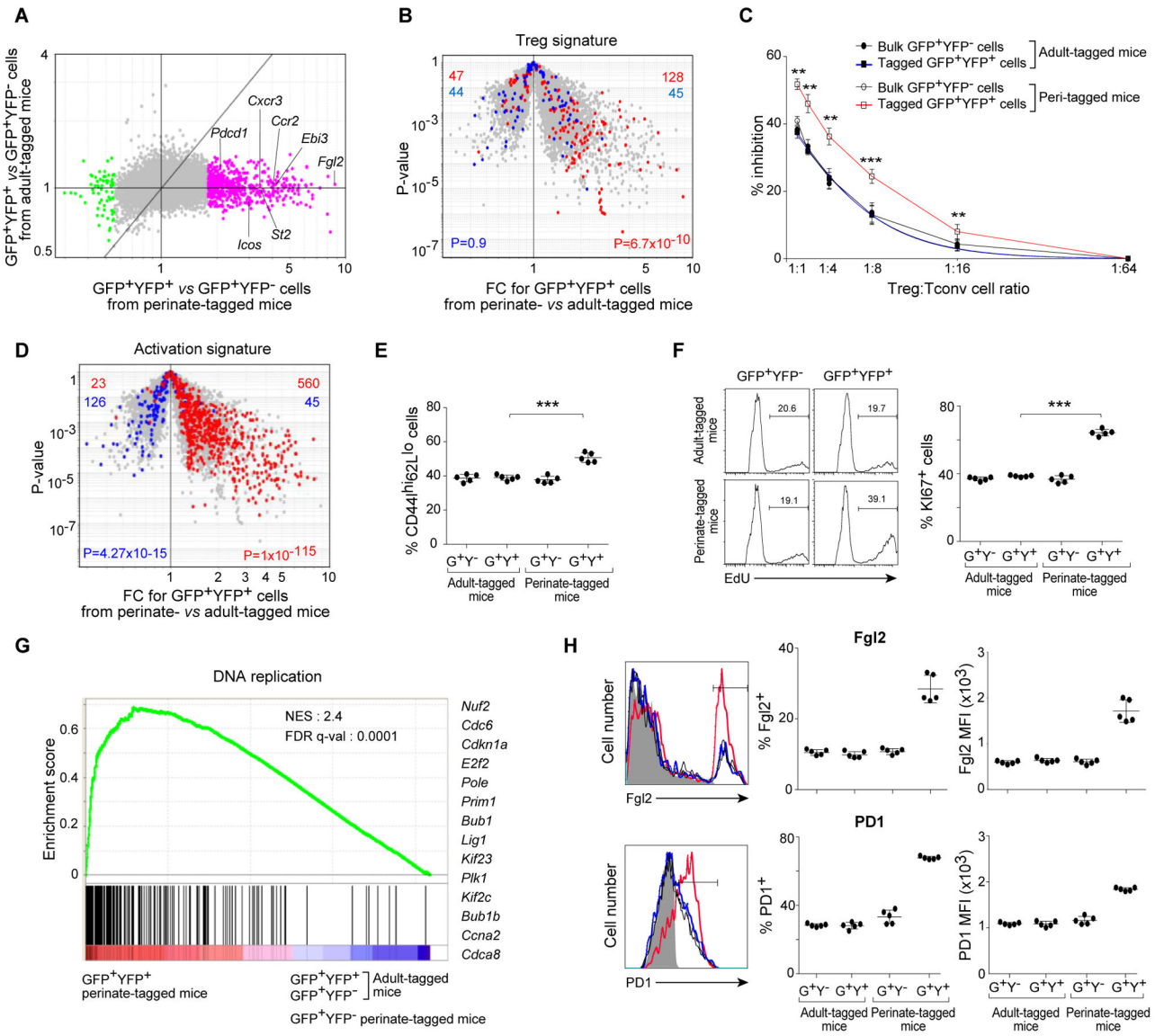

Fig. 3. A distinct transcriptome in perinate-tagged Tregs

The same type of four-way comparison employed in Fig. 2 was conducted except that the sorted cells were analyzed for diverse phenotypic features. **(A)** FC/FC plots comparing perinate-tagged GFP$^+$YFP$^+$ cells vs bulk GFP$^+$YFP$^-$ cells from the same mice (x-axis) and adult-tagged GFP$^+$YFP$^+$ cells vs bulk GFP$^+$YFP$^-$ cells from the same mice (y-axis). Pink dots denote transcripts over-represented in perinate-tagged GFP$^+$YFP$^+$ cells; green dots indicate under-represented transcripts. **(B)** P-value vs FC volcano plot comparing gene expression of perinate-tagged GFP$^+$YFP$^+$ and adult-tagged GFP$^+$YFP$^+$ cells. Red and blue dots indicate up- and down-regulated Treg signature genes, respectively (31). P-values from the chi-squared test **(C)** Classical *in vitro* suppression assay on the four sorted Treg populations. P-values from the Student's t test. **, p≤ 0.01; ***, p≤0.001. **(D)** Same volcano plot as in panel B, except up-(red) and down-(blue) regulated activation signature genes (31) are superimposed. **(E)** Summary data on late activation marker (CD44^{hi}CD62L^{lo})

expression in the four Treg populations. n=5. P-value from the Students' t test ***, P≤0.001. **(F)** EdU uptake (left) and Ki67 expression (right) by the four Treg populations. ***, P≤ 0.001. **(G)** GSEA of transcripts increased in the perinate-tagged GFP^+YFP^+ *vis-à-vis* the adult-tagged control Treg populations. NES, normalized enrichment score. FDR q-val, false discovery rate. Representative transcripts showing increased expression are shown on the right. **(H)** Flow cytometric confirmation of gene over-expression in perinate-tagged Tregs. For Fgl2 and PD1: Left = representative flow-cytometric histograms; red, perinate-tagged; blue, adult-tagged; black, control bulk populations; gray shading, isotype-control antibody; bar indicates marker positivity. Center = summary data for % of the four Treg populations expressing the marker; Right = summary data for marker MFI in the marker-positive population.

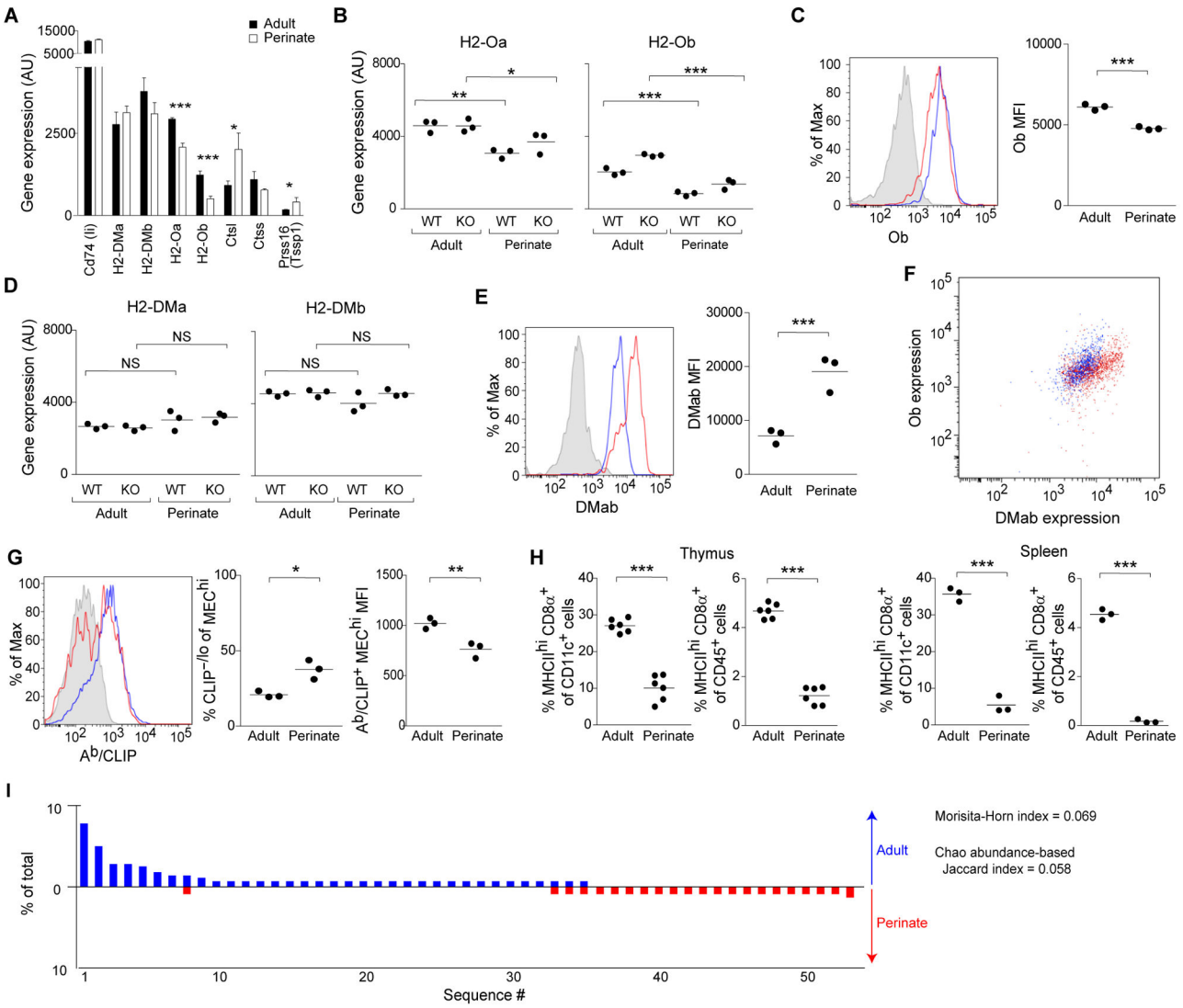

Fig. 4. Age-dependent, Aire-independent differences in the processing and presentation of MEC-generated peptides

(A) Microarray-based quantification of transcripts encoding a set of proteins involved in processing/presentation of MHCII-bound peptides. **(B)** Microarray-based quantification of DOa and DOb in MEC^{hi} from *Aire*-WT or -KO adults or perinates. **(C)** Intracellular expression of DOb protein. Left = representative flow-cytometric histograms. Red, perinate; blue, adult; gray shading, negative control staining. Right = summary MFI data. **(D and E)** Same as panels B and C except DMa and DMb were examined. **(F)** Coordinate intracellular staining of DOb and DMab. **(G)** Surface expression of Ab:CLIP complexes on MEC^{hi}. Left = representive flow-cytometric histograms. Red, perinate; blue, adult; gray shading, negative control staining. Center = summary data for % MEC^{hi} expressing little or no CLIP. Right = summary data for MFI. **(H)** Flow cytometric quantification of MHC^{hi}CD8α^{+} DCs in perinatal vs adult thymus (left) and spleen (right). Summary data for representation in the CD11c^{+} (left) and CD45^{+} (right) compartments. **(I)** High-frequency Vα2^{+} TCRs from 5wk-old (upper) and 4d-old (lower) BDC2.5/NOD females. These sequences correspond to those

in Table S2. Bars represent frequency of each sequence. Except for panel I, P-values are from the Student's t test: *, $P < 0.05$; **, $P < 0.01$; ***, $P < 0.001$. n=3–6.